ACS OMEGA

Article

Cite This: ACS Omega 2019, 4, 104−113

http://pubs.acs.org/journal/acsodf

Synthesis of Positively and Negatively Charged CeO_2 Nanoparticles: Investigation of the Role of Surface Charge on Growth and Development of *Drosophila melanogaster*

Divya Parimi,[‡,†] Vignesh Sundararajan,[§,†] Omer Sadak,[∥] Sundaram Gunasekaran,[∥,⊥] Sahabudeen Sheik Mohideen,[§] and Anandhakumar Sundaramurthy*[,‡,#]

[‡]Department of Physics and Nanotechnology, SRM Institute of Science and Technology, Kattankulathur - 603203, Kanchipuram, Tamil Nadu, India

[§]Department of Biotechnology, SRM Institute of Science and Technology, Kattankulathur - 603203, Kanchipuram, Tamil Nadu, India

[∥]Department of Materials Science and Engineering, University of Wisconsin-Madison, Madison, Wisconsin 53706, United States

[⊥]Department of Biological Systems Engineering, University of Wisconsin-Madison, Madison, Wisconsin 53706, United States

[#]SRM Research Institute, SRM Institute of Science and Technology, Kattankulathur - 603203, Kanchipuram, Tamil Nadu, India

Supporting Information

ABSTRACT: Monodispersed cerium oxide nanoparticles (CeO_2 NPs) with positive and negative surface potential were synthesized by co-precipitation method using hexamethylenetetramine (HMT) and poly(vinylpyrrolidone) (PVP), respectively, as precipitating agents. Synthesized NPs were characterized with scanning electron microscopy (SEM), UV−Visible (UV-Vis) spectroscopy, Fourier transform infrared (FT-IR) spectroscopy, and powder X-ray diffraction (XRD). Positively charged NPs of about 30 ± 10 nm in size formed within 5 h, aggregated in number, and resulted in larger-sized NPs as a function of time. The CeO_2 NPs were administered to *Drosophila* as a part of their diet to study the effects on the growth and development of *Drosophila*. While the positively charged NPs did not affect the growth of the third instar larvae, the negatively charged NPs delayed the growth of larvae by about 7 days. It required 7 more days to reach the stage of adult fly. TEM imaging of the larvae gut showed that positively charged NPs were found to be smaller, whereas the size of negatively charged NPs remained unchanged. This biodegradability could be the reason for the delayed larvae growth in the case of negatively charged particles. The distance covered by such second instar larvae fed with diet containing negatively charged CeO_2 NPs was significantly lower, and their size was significantly smaller when compared to the crawling activity and size of the third instar larvae of the control group. Such positively charged NPs have high potential for use as drug delivery carriers for the treatment of disease, and negatively charged NPs may play a rather detrimental role.

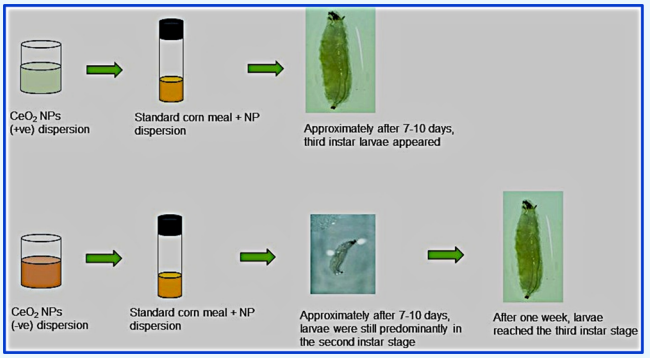

1. INTRODUCTION

Lanthanide elements, such as cerium, are gaining a profound importance in many applications due to their excellent magnetic, optical, electrical, and nuclear properties.[1] Cerium (Ce) and its oxides have received much attention in the fields of physics, chemistry, material sciences, and biology.[2] Their numerous properties are a result of the vacancies in their valance shells, 4f and 5d, which change according to their chemical environment. Cerium oxide (CeO_2) has a cubic fluorite structure, in which each cerium atom is surrounded by eight oxygen atoms in a face-centered cubic (FCC) arrangement, which is stable from room temperature to its melting point of 2400 °C. It is a nonstoichiometric compound and exists in +3 (fully reduced) and +4 (fully oxidized) states, unlike other lanthanide elements that exhibit only the +3 state. The ability of CeO_2 nanoparticles (CeO_2 NPs) to switch between their dual oxidation states (+3 and +4) affords those properties, such as the ability to store and transport oxygen,[3] ability to absorb UV light,[4] high thermal stability,[5] electrical conductivity and diffusivity,[6] high hardness, and specific chemical reactivity.[7]

CeO_2 NPs are prepared by various methods including hydrothermal process,[8] sol−gel precipitation,[9] microemulsion process,[10] solvothermal synthesis,[11] spray pyrolysis, etc.[12] Most

Received: October 10, 2018
Accepted: December 18, 2018
Published: January 2, 2019

DOI: 10.1021/acsomega.8b02747
ACS Omega 2019, 4, 104−113

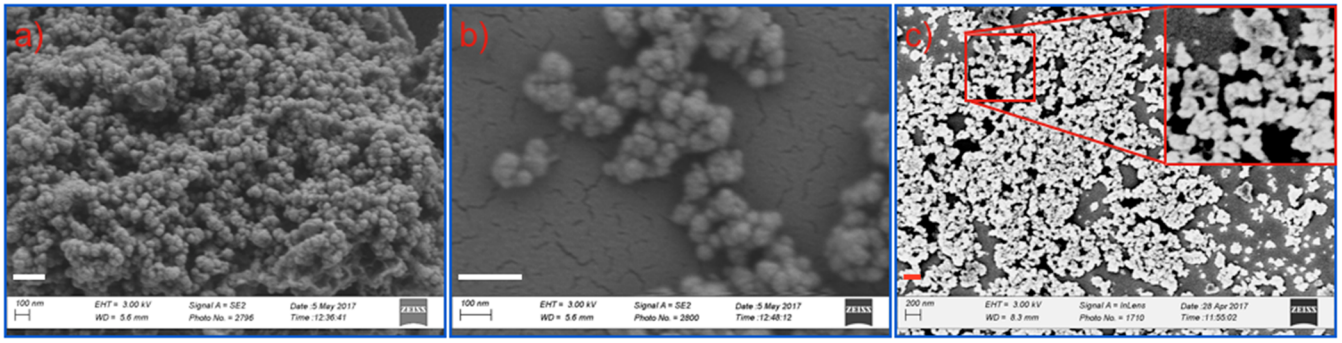

Figure 1. (a–c) SEM images show the morphology of positively charged CeO_2 NPs as a function of reaction time: (a) 5 h, (b) 8 h, and (c) 20 h. Inset in image (c) shows NPs at higher magnifications (Scale bar = 200 nm).

of these methods involve the use of high temperature and pressure and are difficult to control. For instance, solvothermal method requires expensive equipment and longer reaction time and poses safety concerns during reaction.[11] Other drawbacks, such as the formation of submicrometer-sized particles, polydispersed amorphous NPs, and the presence of impurities, limit their use in the synthesis of CeO_2 NPs for biological applications.[13−15] As a result, various surfactant molecules that could directly reduce the Ce precursor salts into CeO_2 NPs by co-precipitation at room temperature and under benign conditions are being continuously explored. Previous reports show that CeO_2 NPs can be easily prepared by co-precipitating $Ce(NO_3)_3{\cdot}6H_2O$ using poly(vinylpyrrolidone) (PVP) or poly(ethylene glycol) (PEG) under basic conditions.[16] However, the particles obtained were aggregated and polydispersed with a size range of about 10−50 μm. By using hexamethylenetetramine (HMT) as a surfactant, stable CeO_2 NPs with a size ranging from 2.6 to 240 nm were prepared by increasing the reaction time.[17] Although the study claims that size of the NPs increased as a function of time, there is no information about the NP growth whether NPs are growing continuously or undergo secondary aggregation during the growth process. Moreover, the surface charge of NPs and its use in biological applications need to be investigated in detail.

Various attempts have been made to exploit the uniqueness of CeO_2 NPs in switching the oxidation states between +3 and +4 and vice versa in biological applications as CeO_2 NPs can act as analogues to natural antioxidants. In biological systems, cells under oxidative stress produce many reactive oxygen species (ROS) such as superoxide anion radical ($O_2^{\cdot}$), hydroxyl radical ($^{\cdot}OH$), singlet oxygen (O_2), and hydrogen peroxide (H_2O_2).[18] These ROS are highly reactive compounds and have the potential to damage and impair cell functioning. CeO_2 NPs with +3 oxidation state can transmute ROS species into H_2O and O_2 in two steps (ROS to H_2O_2 to $H_2O + O_2$) by changing its oxidation state to +4.[18] As these scavenging activities mimic the role of superoxide dismutase (SOD) and catalase enzymes found in living systems,[19] CeO_2 NPs have been widely investigated for their antioxidant and protective effect against cell damage caused by ROS,[20] hydrogen peroxide,[21] radiation,[22] and antigenotoxic effect against potassium dichromate-induced genotoxicity.[23] Thus, the widespread use of CeO_2 NPs warrants the investigation of its potential toxicity in in vivo models.

Among the reports discussed about the cytotoxicity of CeO_2 NPs in living systems, in vitro toxicological investigations on human (mesothelioma MSTO 211H) and rodent (3T3 fibroblast cells) cell lines showed that short-term exposure to CeO_2 NPs imparted cytotoxicity on cells; however, the cells recovered gradually 6 days after exposure.[24] Similarly, a study on inflammatory response of CeO_2 NPs on human aortic endothelial cells (HAECs) showed that NPs were benign and did not cause inflammation in HAECs even at high concentrations.[25] Investigations of CeO_2 NPs with different surface charges showed that positively charged particles favored protein adsorption while negatively charged particles were found to be internalized inside the cells.[26] However, in vitro studies using positively and negatively charged CeO_2 NPs elicited contrasting effects. Asati et al. reported that the toxicity elicited by CeO_2 NPs after its subcellular localization was based on its surface charge. In cancer therapy, CeO_2 NPs localized in lysosomes exhibited significant cytotoxicity, whereas NPs localized in the cytoplasm exhibited minimal cytotoxicity. Positively charged CeO_2 NPs were toxic to all cancer cells except breast cancer cells due to its localization into lysosomes, and negatively charged CeO_2 NPs were toxic only to A459 lung cancer cells. The neutrally charged CeO_2 NPs were nontoxic to both normal and cancer cells as it was localized primarily in the cytoplasm of the cells. Interestingly, negatively charged CeO_2 NPs were not internalized by normal cells and hence were nontoxic.[27] The toxicity of CeO_2 NPs was also studied in honeybees. Kos et al. investigated the effect of oral ingestion of CeO_2 NPs (2−500 mg/L) along with food on summer and winter honeybees after 9 days of exposure. The highest dose (500 mg/L) of CeO_2 NPs had no effect on the survival of honeybees. However, both the summer and winter honeybees exhibited alterations in biochemical parameters such as acetylcholinesterase (AChE) and glutathione *S*-transferase (GST).[28] Only a few studies have investigated the effect of CeO_2 NPs in *Drosophila melanogaster* apart from in vitro models, and it was reported that nanoceria exerted a protective effect against free-radical-mediated toxicity.[29,30] Moreover, CeO_2 NPs also elicited beneficial effects in *Drosophila* by increasing its lifespan by 38% and a 200% increase in survival after exposure to a lethal dose of paraquat.[29,31] Female flies were benefited more by the administration of CeO_2 NPs as evidenced by the increase in median lifespan and maximum lifespan by 18 and 19 days, respectively.[30]

This application of CeO_2 NPs is also in concordance with the work on effects of CeO_2 NPs on differentiated SH-SY5Y human neuroblastoma cells (neuronal model) for Alzheimer's disease research. CeO_2 NPs exhibit both neurotrophic role in protecting the cells against amyloid-β (Aβ) injury and in Aβ-induced oxidative stress[32] and neuroprotective activity in an in

DOI: 10.1021/acsomega.8b02747
ACS Omega 2019, 4, 104−113

vitro mouse hippocampal brain slice model of ischemia.[33] The neuroprotective effects of CeO_2 NPs has also been reported in a mouse model of 1-methyl-4-phenyl-1,2,3,6-tetrahydropyridine (MPTP)-induced Parkinson's disease. CeO_2 NPs at 0.5 μg/g were most effective in elevating the striatal dopamine content and the numbers of TH+ neurons.[34] Negatively charged nanoceria with a zeta potential of −18.2 mV shows antigenotoxic and antioxidant properties and is nontoxic up to a concentration of 10 mM in *Drosophila*.[23] *Drosophila* is widely used as an in vivo model to study the biological effects as well as the toxicity of NPs[35−37] since 75% of its genes are analogous to the human disease-related genes. To the best of our knowledge, there are no studies till date in *Drosophila*, investigating the effect of charged nanoceria. In the present work, we used co-precipitation method to synthesize negatively and positively charged CeO_2 NPs by reducing $Ce(NO_3)_3$ with PVP and HMT, respectively. Attempts have been made to synthesize stable CeO_2 NPs with a size range of 10−20 nm, and particle growth mechanisms have been investigated in detail. NPs with positive and negative surface charge were fed to *Drosophila melanogaster*, and the growth and distance covered by larvae were investigated to use the synthesized NPs for the treatment of Alzheimer's disease.

2. RESULTS

2.1. Preparation of CeO_2 NPs. Both positively (using HMT) and negatively (using PVP) charged CeO_2 NPs were stable and spherical with the size range of about 20−30 nm (Figures 1−4). When HMT was used as a precipitating agent,

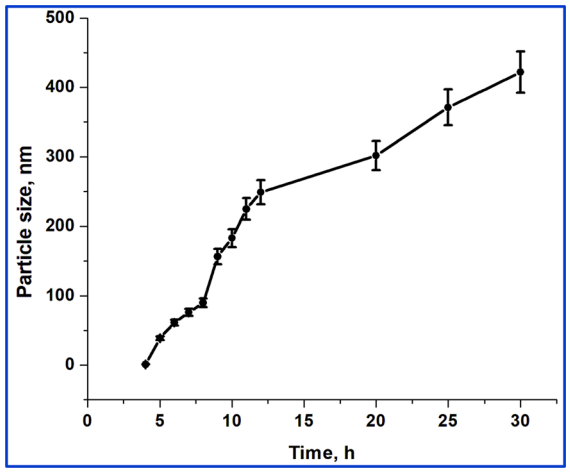

Figure 2. Dynamic light scattering measurements show the growth of HMT-stabilized CeO_2 NPs as a function of time (Figures S3−S5, Supporting Information).

the particle size increased as a function of time, reaching a maximum of about 450 ± 30 nm (Figure 2). The size and surface potential of synthesized NPs are as shown in Figure 5. The NPs stabilized with HMT and PVP showed a potential of +27.6 and −32.9 mV, respectively. Notably, synthesis of the NPs with either surfactant yielded in differently charged cerium oxide NPs. The surface potential of >25 mV along with a sharp single peak showed that the NPs formed were monodispersed and stable. These studies give us knowledge on the accumulation of differently charged ions on the surface of the NPs along with their specific potential.

2.1.1. UV−Visible spectroscopy. UV−Vis absorption spectra depicted in Figure 6 revealed strong absorption peaks in the range between 280 and 300 nm, which are the specific characteristic peaks of CeO_2 NPs.

2.1.2. FT-IR Spectroscopy. The FT-IR spectrum of CeO_2 NPs synthesized with HMT shows three characteristic peaks centered at 716, 2920, and 1500 cm^{-1}, which correspond to the rocking, stretching, and bending vibrations, respectively, of the methyl groups of hexamine (Figure 7). It is worth noting that rocking vibrations at 716 cm^{-1} is the characteristic peak for a minimum of four methyl groups in a row, that is, $(CH_2)_6$ groups of HMT. The peaks observed at 1650 and 3468 cm^{-1} correspond to hydrogen-bonded O—H groups and stretching vibrations of water molecules. The peak centered at ∼500 cm^{-1} is the characteristic peak for the formed cerium oxide NPs. The spectrum of CeO_2 NPs synthesized with PVP shows three characteristic peaks at 3350, 1720, and 1620 cm^{-1}, which correspond to O—H groups of water molecules and C═O stretching and C═C vibrations of PVP, respectively. The peaks at 2920, 1455, 1380, and 1290 cm^{-1} correspond to CH_2 stretching, C—H deformation, CH_3 symmetrical deformation or CH_2 bending, and C—N stretching, respectively. The characteristic peak of CeO_2 was observed at ∼480 cm^{-1}.

2.1.3. XRD Investigations. Despite the fact that both patterns were in concordance with standard patterns of CeO_2 NPs (JCPDS card no. 34-0394), XRD patterns of both NPs appeared to be distinct, which are shown in Figure 8. Notably, XRD peaks of negatively charged NPs were sharp, which implies that the formed particles are precisely crystalline and also match with the cubic fluorite structure of CeO_2 with miller indices (111), (200), (220), (311), (222), (400), (331), and (420) at 28.5°, 33.08°, 47.47°, 56.3°, 69.4°, 76.7°, and 79.07°, respectively, whereas the XRD patterns of positively charged particles also included peaks of secondary structures of CeO_2 NPs with miller indices (100), (002), (101), (102), (110), and (202) at 24.4°, 27.4°, 30.3°, 38.5°, 45.2°, and 63°, respectively (JCPDS card no. 23-1048).

2.2. Investigation of CeO_2 NPs in *Drosophila melanogaster*. *2.2.1. Effect of CeO_2 NPs on Larval Development.* For larval development investigations, the size of positively and negatively charged NPs used was 30 ± 10 and 20 ± 10, respectively. The third instar larvae that emerged after 7−10 days from the treatment groups were observed under a stereomicroscope. While the larvae that fed on control and positively charged CeO_2 NP-containing cornmeal diet did not exhibit any delayed development and reached the third instar stage in 8 days, the larvae that fed on negatively charged CeO_2 NP-containing diet exhibited delayed development and reached the third instar stage only after 15 days (Figure 9). This adverse effect of negatively charged NPs was further investigated using TEM/HR-TEM imaging in Figure 10. Notably, negatively charged NPs found in gut samples were similar in size and morphology when compared to as-prepared NPs, whereas the positively charged NPs were found to be smaller in size in the gut, which can be due to biodegradation in the larvae gut. It is believed that the larvae degrade positively charged NPs at a higher rate than that of negatively charged NPs. The lower rate of degradation of the negatively charged NPs can be pointed out as the factor that influenced the delay in larvae development. This suggests that the negatively charged CeO_2 NPs causes the delay in the development of the third instar larvae. However, no defects in pupa formation were seen, and third instar larvae stopped feeding to become pupae

DOI: 10.1021/acsomega.8b02747
ACS Omega 2019, 4, 104−113

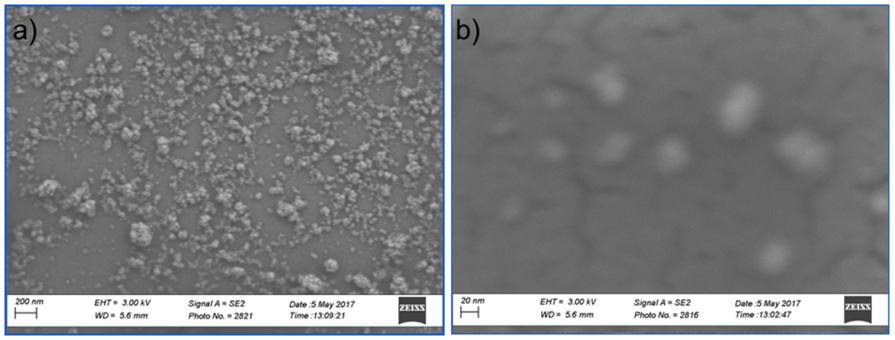

Figure 3. (a, b) SEM images show the morphology of negatively charged CeO_2 NPs prepared by precipitation of $Ce(NO_3)_3$ with PVP. Images show negatively charged NPs at (a) lower and (b) higher magnifications.

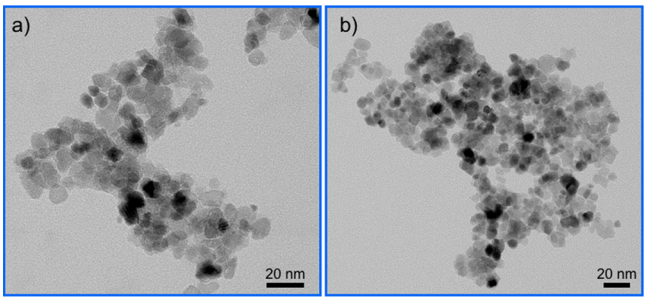

Figure 4. (a, b) TEM images show the morphology of (a) positively and (b) negatively charged CeO_2 NPs after 5 h of reaction.

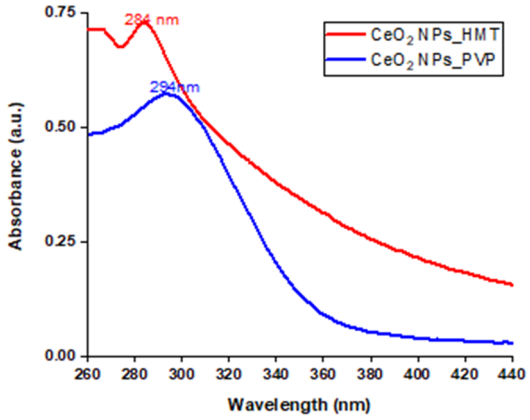

Figure 6. UV−Vis spectra of CeO_2 NPs prepared by HMT (in red, with a peak at 284 nm) and NaOH/PVP (in blue, with a peak at 294 nm).

after reaching the third instar stage. Moreover, no phenotypic defects were seen in the adult flies that hatched from the third instar larvae from the positively and negatively charged NP-containing food.

2.2.2. Effect of CeO_2 NPs on Larval Growth. The length and breadth of each larva was measured, and statistical analysis was performed, as shown in Scheme 1 and Figure 11. While there was no statistical significance in the length and breadth of positively charged CeO_2 NP-fed larvae, the larvae that fed on cornmeal diet containing negatively charged CeO_2 NPs exhibited a significant decrease ($P < 0.05$) in length at a dose of 1 mM and in breadth at both doses [0.1 mM ($P < 0.05$) and 1 mM ($P < 0.001$)]. However, the length and breadth of the larvae when they reached the third instar stage after a week were not statistically significant at both 0.1 and 1 mM doses (Figure 11).

2.2.3. Crawling Assay. The larval crawling assay was performed to assess the extent of neuronal damage as the crawling activity is under the control of motor neurons present in the ventral ganglion.[38] The distances covered by the larvae of control, 0.1 mM (A), 1 mM (A), 0.1 mM (B), and 1 mM (B) were 43.40, 49.81, 45.07, 30.18, and 26.51 mm/min, respectively (Figure 12). Compared to control, a statistically significant decrease in the distance covered by the larvae was observed at 0.1 mM ($P < 0.001$) and 1 mM ($P < 0.0001$) doses of the negatively charged CeO_2 NPs, and this indicates that the negatively charged NPs affected the crawling activity of the third instar larvae.

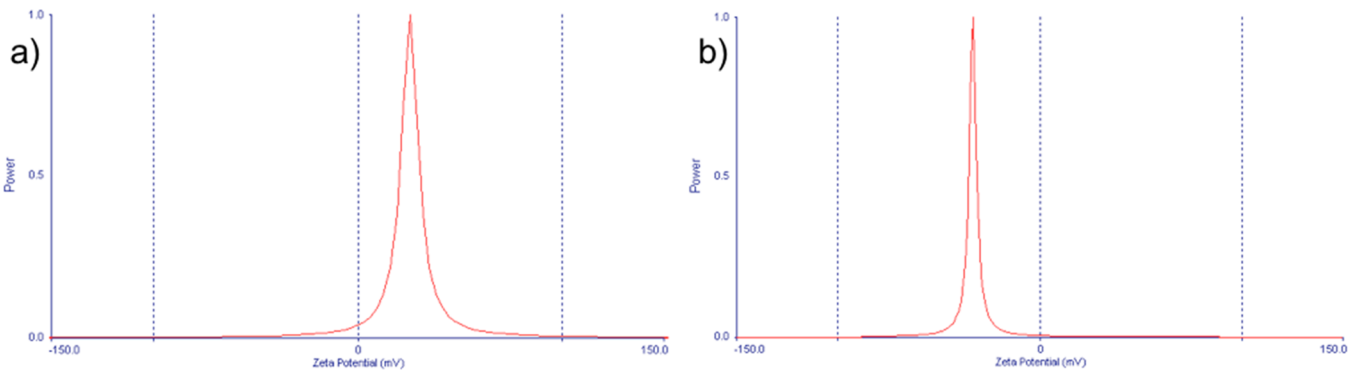

Figure 5. (a, b) Zeta potential of as-prepared (a) positively charged (with HMT) and (b) negatively charged (with PVP) CeO_2 NPs.

DOI: 10.1021/acsomega.8b02747
ACS Omega 2019, 4, 104−113

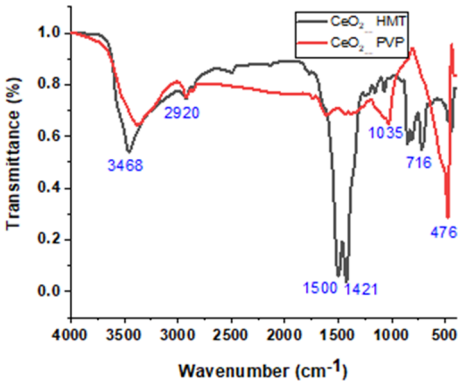

Figure 7. FT-IR spectra of CeO_2 NPs prepared with HMT and PVP.

3. DISCUSSION

3.1. Synthesis of Positively and Negatively Charged CeO_2 NPs. CeO_2 NPs with positive and negative surface potential were prepared by co-precipitation of $Ce(NO_3)_3 \cdot 6H_2O$ with HMT and PVP. Synthesis with HMT is a single-step process, and the size of NPs increased as a function of time. Initially, the reactant suspension was clear in the first 2 h and turned into turbid as a function of time. This inference was supported by performing time-dependent growth studies of the NPs as shown in Figure 2. The formation of the NPs by using HMT is dependent on the duration of the synthesis process, and the size of NPs is not constant at any two different time intervals throughout the process. The estimated particle size was about 3 nm after 3 h, which increased to 30 ± 10 nm after 5 h. When the reaction continued, the size of the particles increased continuously and reached about 440 ± 30 nm after 30 h. It is believed that the formation of the NPs was completed at the early hours of the synthesis, but as the time progresses, NPs tend to aggregate in number, resulting in larger-sized particles. To get more detailed information about the NP growth, the formed NPs were investigated with SEM, TEM, and dynamic light scattering (DLS), as shown in Figures 1−4. Investigations showed that NPs were spherical with a size range of about 30 ± 10 nm after 5 h. Although size measurements showed that the size of NPs increased as a function of time, morphological investigations proved that NPs of 30 ± 10 nm in size underwent secondary aggregation and resulted in NP growth as a function of time. Attempts to disperse the aggregated NPs using ultrasound were not successful in dispersing the NPs. It can be concluded that NPs grow up to 5 h and undergo secondary aggregations when the reaction was allowed to continue (Scheme 2). On the other hand, synthesis with PVP is a two-step process: (1) transformation of $Ce(NO_3)_3 \cdot 6H_2O$ into cerium hydroxide, and (2) calcination of cerium hydroxide into CeO_2 NPs at 600 °C for 2 h. The precursor ions (Ce^{3+}) react with the hydroxyl ions (OH^-) from NaOH and form cerium hydroxide NPs ($Ce(OH)_4$) as an intermediate compound, which, upon calcination under atmospheric conditions, oxidizes into CeO_2 NPs.[16] The NPs were spherical, and the size was found to be about 20 ± 10 nm. Notably, NPs synthesized with HMT and PVP showed a surface potential of +27.6 and −32.9 mV, respectively (Figure 5). The surface potential of greater than ±25 mV along with a sharp single peak indicated that the NPs formed were monodispersed and stable. In the PVP-assisted process, the calcination at 600 °C resulted in the removal of PVP from the NPs. Hence, the monodispersity and the controlled size of the NPs were approximated due to the accumulation of sodium nitrate ($NaNO_3$) ions onto the surface of NPs.[39]

To get more detailed information about the NP formation, phases present, and crystallinity, the synthesized NPs were characterized with UV−Vis spectroscopy, FT-IR, and XRD. UV−Vis investigations show that both NPs revealed strong absorption peaks in the range between 280 and 300 nm, which is a specific characteristic peak of cerium oxide NPs (Figure 6). It was reported that a red shift in the absorption peak of PVP-stabilized CeO_2 NPs was influenced by the quantity of Ce^{3+}/Ce^{4+} present in the NPs.[40] XRD investigations confirmed that the XRD patterns of synthesized NPs matched well with the standard patterns of cerium oxide NPs (JCPDS card no. 34-0394), as shown in Figure 8. Notably, XRD peaks of the negatively charged particles were sharp, which elucidated that the formed particles were precisely crystalline and also in accordance with the cubic fluorite structure of CeO_2 NPs with miller indices (111), (200), (220), (311), (222), (400), (331), and (420) at 28.5°, 33.08°, 47.47°, 56.3°, 69.4°, 76.7°, and 79.07°, respectively, whereas the XRD patterns of positively charged particles also included peaks of secondary structures of cerium oxide (JCPDS card no. 23-1048). These variations in the structures of the NPs were believed due to heat treatment of the NPs during the synthesis process. The negatively charged NPs were calcined at higher temperatures (600 °C), which aided the NPs to be more crystalline, whereas the positively charged NPs were only exposed to low temperatures (50−60 °C), which paved a way to form secondary structures.

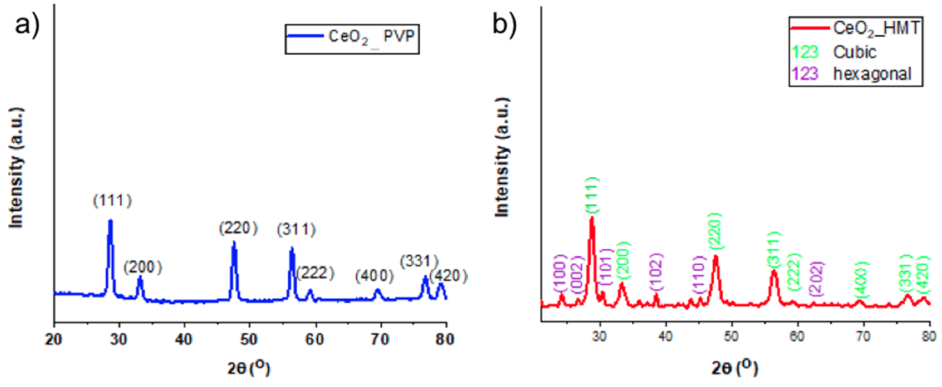

Figure 8. (a, b) XRD patterns obtained on CeO_2 powders prepared by homogeneous precipitation of $Ce(NO_3)_3$ with (a) NaOH/PVP calcined at 600 °C and (b) HMT at room temperature.

DOI: 10.1021/acsomega.8b02747
ACS Omega 2019, 4, 104−113

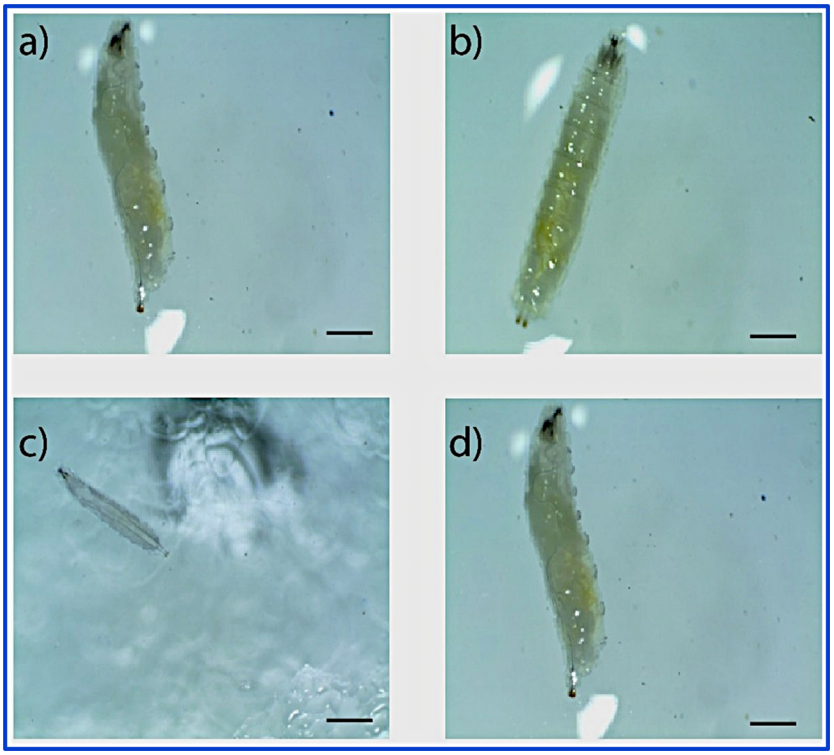

Figure 9. (a–c) Images of larvae fed with (a) cornmeal diet control (b) with positively charged CeO_2 NPs and (c) with negatively charged CeO_2 NPs after 7 days. (d) Image of larvae fed with cornmeal diet containing negatively charged CeO_2 NPs after 15 days. This indicates that negatively charged NPs delay the growth by 1 week. Scale bar = 500 μm.

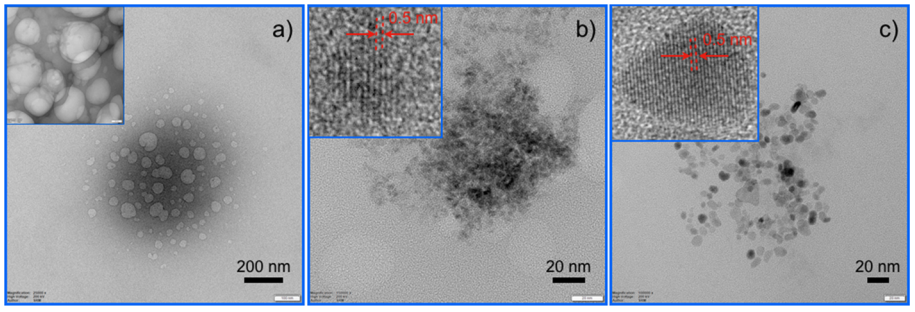

Figure 10. (a–c) TEM investigations show the presence of CeO_2 NPs in the larvae gut. Larvae fed with (a) control (normal) and (b) positively charged and (c) negatively charged NP-containing food. Insets show corresponding images at higher magnifications. It is noteworthy that lattice fringes of CeO_2 NPs are clearly visible in insets of (b) and (c).

3.2. Investigation of Positively and Negatively Charged CeO_2 NPs on Growth and Development of *Drosophila melanogaster*. The positively charged NPs did not elicit any morphological alterations and delay in the growth of *Drosophila*. The length and breadth of the larvae from this treatment group were comparable to those of the control group, without any statistical significance. Both the control and positively charged treatment groups became third instars at the same time, and new flies were observed simultaneously. Moreover, the crawling activity of the larvae was also not affected. However, the larvae that fed on food containing negatively charged NPs exhibited morphological alterations and decreased crawling speed. Since there are no previous in vivo studies with charged CeO_2 NPs to correlate the findings of the present study, more studies are warranted to further investigate how the surface charge of CeO_2 NPs elicits delayed development in *Drosophila*. However, based on the available literature regarding the effect of surface charge of NPs and its uptake and toxicity, it can be postulated that the delayed development observed in larvae that fed on food containing negatively charged NPs could be due to decreased cell–NP interaction, and subsequently, it reduced cellular uptake of food ingredients along with the NPs, and thereby, no degradation was observed (Figure 10). El Badawy et al. reported that in Gram-positive bacteria, a strong cell–NP repulsion was observed due to the presence of a negative charge on the cell membrane of bacillus cells and negatively charged citrate-capped silver NPs. With positively charged NPs, the repulsion decreased and cell–NP interaction increased.[41] Moreover, it has been reported that compared to neutrally charged iron oxide NPs (coated with PEG), positively charged iron oxide NPs (coated with polyethylenimine) exhibited enhanced cellular uptake, faster blood clearance, and dose-dependent cytotoxicity.[42] A study performed in pregnant mice also reported that compared to negatively charged iron oxide NPs, iron oxide NPs coated with

DOI: 10.1021/acsomega.8b02747
ACS Omega 2019, 4, 104–113

Scheme 1. Schematic Representation of the Effect of Surface-Charged CeO_2 NPs on the Growth and Development of Third Instar Larvae

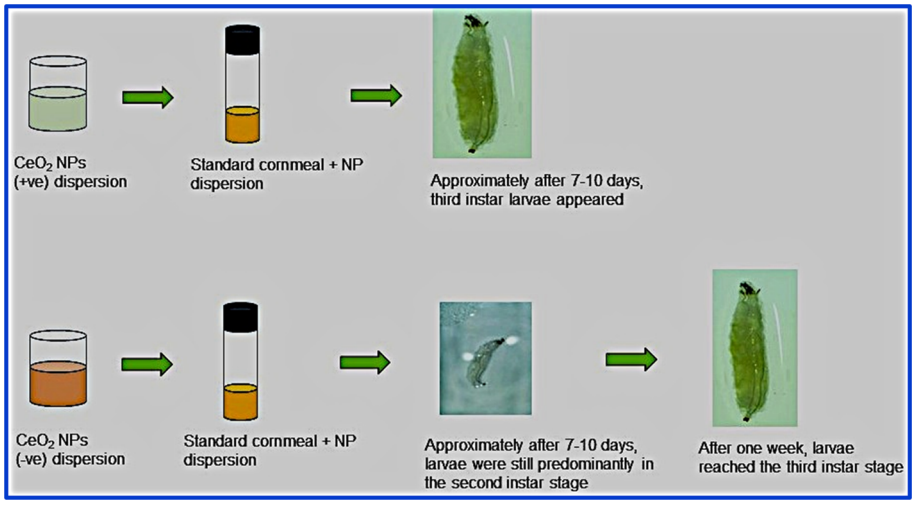

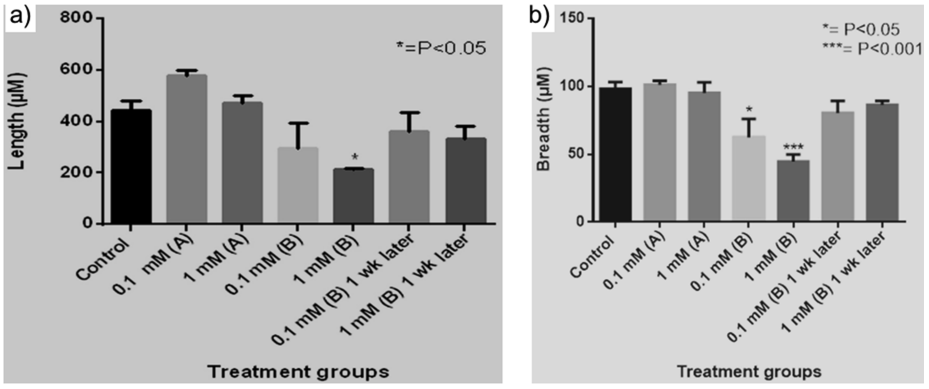

Figure 11. Effect of positively and negatively charged CeO_2 NPs on the length (left) and breadth (right) of *Drosophila*. (a) Positively charged and (b) negatively charged CeO_2 NPs at two concentrations. The values represented are mean ± SEM (n = 3). Statistical significance was set to P < 0.05, and significant values indicate a decrease in length/breadth when compared to control.

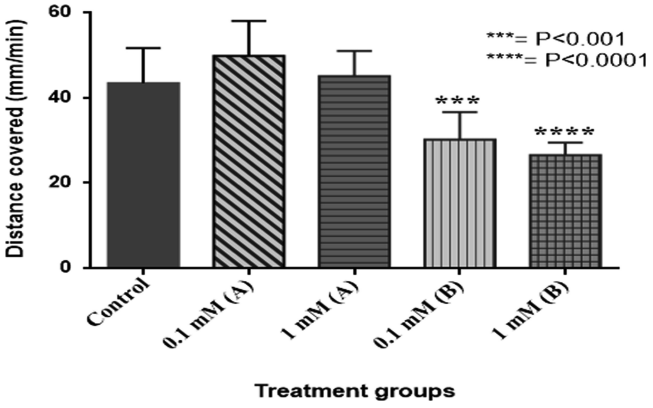

Figure 12. Distance covered by larvae that fed on control, (A) positively charged CeO_2 NPs, and (B) negatively charged CeO_2 NP-containing food. The values represented are mean ± SEM (n = 9). Statistical significance was set to P < 0.05, and significant values indicate a decrease in distance covered by larvae when compared to control.

positively charged polyethylenimine exhibited increased bioaccumulation of iron in the fetal liver,[43] suggesting the preferential uptake of positively charged NPs by cells. As toxicity is based on NP localization in the cell, positively and

Scheme 2. Schematic Illustration showing the Nanoparticle Growth Mechanism in HMT-Assisted Synthesis Process

negatively charged NPs are taking different routes to reach the lysosome and cytoplasm, respectively. Notably, toxicity was high for positively charged NPs localized at the lysosome than that of negatively charged NPs localized at the cytoplasm. Investigation of CeO_2 NPs in cancer cells showed that positively charged NPs were toxic to all cancer cells except breast cancer cells because of its localization in lysosomes, whereas negatively charged NPs were toxic only to A459 lung cancer cells. Interestingly, neutrally charged cerium oxide NPs also accumulated in the cytoplasm and induced no cytotoxicity to both normal and cancer cells. Since the larvae that fed on negatively charged NPs exhibited delayed development, it is believed that the negatively charged CeO_2 NPs were internalized by larval cells. Previous reports claimed that although positively charged NPs favored protein adsorption, NPs were not effectively internalized in A459 lung cancer cells

DOI: 10.1021/acsomega.8b02747
ACS Omega 2019, 4, 104−113

and induced no cytotoxicity. In the present study, we did not observe any phenotypic defects in the body parts of adult flies that hatched from third instar larvae, such as head, eyes, wings, legs, and abdomen, for both the positively and negatively charged groups. This is in accordance with the results of a previous study, except for scutellar bristles, using negatively charged CeO_2 NPs with a zeta potential of −18.2 mV.[23] Although the authors mentioned the lack of toxicity up to a dose of 10 mM, there is no mention of any delayed development of the larvae, and the results obtained in our study shed a new dimension on the effect of negative surface charge. This might be due to the difference in the approach used to synthesize negatively charged CeO_2 NPs and, more importantly, the inability to biodegrade the negatively charged CeO_2. Since the positively charged CeO_2 NPs did not elicit any developmental delay and favored BSA adsorption, it is proposed to use the positively charged CeO_2 NPs at a dose of 0.1 mM in future studies as a drug delivery agent. On the other hand, negatively charged NPs were internalized effectively and resulted in delayed growth for about a week. Hence, the current study has provided important information regarding the effect of surface charge of CeO_2 NPs on the growth and development of *Drosophila*.

4. CONCLUSIONS

We synthesized positively and negatively charged CeO_2 NPs by co-precipitation method using HMT and PVP, respectively, as precipitating agents. Positively charged NPs of about 30 ± 10 nm in size tend to aggregate in number, resulting in larger-sized NPs as a function of time. The addition of PVP into the solution of cerium nitrate at basic pH resulted in negatively charged CeO_2 NPs after calcination at 600 °C. The nitrates formed from the reaction tend to mask the negatively charged NPs and prevent them from agglomeration, resulting in spherical monodispersed NPs of about 20 ± 10 nm in size. Negatively charged CeO_2 NPs are precisely crystalline and arranged in the cubic fluorite structure of cerium oxide. The positively charged NPs do not affect the growth and development of *Drosophila* and can be used in future studies as a drug delivery agent. The negatively charged NPs caused a delay in larve development by 1 week, due to its non-degradable nature. The detailed mechanistic insights in the uptake process of NPs resulting from the current study will be highly valuable for the design of drug delivery systems for the treatment of Alzheimer's disease.

5. EXPERIMENTAL SECTION

5.1. Chemicals. Cerium nitrate hexahydrate ($Ce(NO_3)_3 \cdot 6H_2O$) (HMT), sodium hydroxide (NaOH), poly-(vinylpyrrolidone) (PVP), D-glucose, and yeast extract powder were purchased from SRL Pvt. Ltd., India. Agar-agar type I, propionic acid, methyl parahydroxybenzoate, and orthophosphoric acid were purchased from HiMedia (Mumbai), Merck Life Sciences (Mumbai), Rankem (New Delhi), and Thermo Fischer Scientific (Mumbai), respectively. All chemicals were of analytical grade and used as received. Milli-Q water with a resistivity of >18.2 MΩ·cm was used for all experiments.

5.2. Synthesis of CeO_2 NPs. Positively charged CeO_2 NPs were synthesized as reported previously via aqueous precipitation method using HMT.[17] Briefly, 100 mL of 0.1 M solutions of cerium nitrate hexahydrate and HMT were separately prepared in water. Later, HMT solution was added drop by drop into cerium nitrate hexahydrate solution under stirring (Scheme 3). This mixture was left for 30 h at

Scheme 3. Schematic of the Synthesis of Negatively Charged CeO_2 NPs by Reducing $Ce(NO_3)_3$ with PVP and That of Positively Charged CeO_2 NPs by Reducing $Ce(NO_3)_3$ with HMT

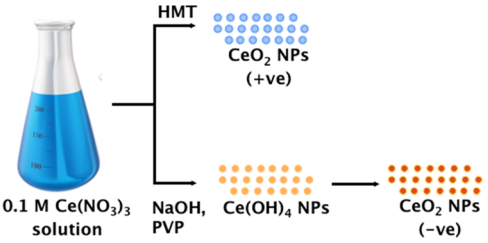

room temperature under continuous stirring at 400 rpm. At predetermined time points, 2 mL of the sample was withdrawn, washed with Milli-Q water, and investigated in DLS. After completion of the reaction, the suspension was centrifuged at 9000 rpm for 20 min and washed five times with water. Finally, the formed pellet was dried overnight in an oven at 50 °C to obtain CeO_2 NPs.

Negatively charged CeO_2 NPs were synthesized by aqueous precipitation of cerium nitrate hexahydrate using PVP.[16] Briefly, 100 mL of 0.4 M sodium hydroxide (NaOH), 100 mL of 0.1 M cerium nitrate hexahydrate, and 2 mL of 10% PVP solutions were prepared separately in water. The original procedure was modified slightly to obtain monodispersed stable NPs. In the original procedure, cerium nitrate solution was added drop by drop to the mixture of PVP and NaOH solution, which resulted in microparticles of about 10−50 μm in size.[16] In the present work, NaOH solution was first added drop by drop to 100 mL of 0.1 M cerium nitrate hexahydrate solution under stirring at 1000 rpm, followed by the addition of 2 mL of PVP solution. After 1 h of reaction, a yellow-colored precipitate was observed, which was due to the formation of cerium hydroxide NPs. This precipitate was centrifuged at 10,000 rpm for 20 min and washed with Milli-Q water and ethanol (5−10 times) to remove any leftover reactants. The pellet was dried for 24 h at 60 °C and calcined at 600 °C for 2 h to oxidize cerium hydroxide particles into CeO_2 NPs.

5.3. Fly Strains and Culture. The wild-type *Drosophila* strain (Oregon K) was used in this study. They were reared at 25 ± 1 °C, 60% humidity, and a 12 h dark-light cycle on a standard cornmeal diet consisting of corn flour, D-glucose, sugar, agar-agar type 1, and yeast extract powder. Antifungal agents such as propionic acid, methyl paraben, and orthophosphoric acid were added to the cornmeal diet at 55 °C after autoclaving to prevent the growth of fungus.

5.4. Experimental Setup for Biological Studies. The experimental setup consisted of three series of control, 0.1 mM, and 1 mM of both positively charged (denoted as "A") and negatively charged (denoted as "B") CeO_2 NPs/mL of food in vials, each containing 6 mL of the cornmeal agar. An aqueous dispersion of CeO_2 NPs (30 mM) in Milli-Q water was prepared by sonication in a water bath to obtain a uniform dispersion. The stock dispersion was diluted to obtain the desired concentrations and added to the food. After 24 h, 25 female and 10 male flies were each transferred to the vials for

DOI: 10.1021/acsomega.8b02747
ACS Omega 2019, 4, 104−113

mating and discarded after 48 h. The third instar larvae that emerged from such food vials were used for the studies.

5.5. Stereoscopic Microscopy. To assess the effect of CeO_2 NPs on larval growth and development, third instar larvae from the control and positively charged CeO_2 NPs treated groups were observed under a stereomicroscope to observe for defects in growth and development. For the negatively charged CeO_2 NPs group, photos of larvae were taken before and after they reached the third instar stage. Briefly, three larvae from each vial were immobilized on ice, and their images were taken under a stereomicroscope at 20× magnification. The length and breadth of the larvae were measured, and statistical analysis was performed to assess the significant differences between the groups. The phenotype of flies that hatched from the third instar larvae was also observed for any phenotypic changes.

5.6. Larval Crawling Assay. The larval crawling assay was performed based on a previously described method.[44] Nine third instar larvae from the control and treatment groups were collected, washed with 1× PBS to remove any food traces, and transferred onto a glass Petri plate coated with 2% agarose. The larvae were allowed to crawl on the agarose surface placed over a graph sheet three times and were filmed. The number of grid lines crossed in 1 min was counted, and the mean distance covered for each group of nine larvae (mm/min) was calculated.

5.7. Characterization. *5.7.1. UV-Vis Spectroscopy.* A small amount of the as-prepared NP powder was dispersed in water and used to obtain the UV−Vis absorption spectra of the CeO_2 NPs in a Nanodrop 2000c spectrophotometer in the wavelength range of 200−750 nm.

5.7.2. Fourier Transform Infrared (FT-IR) Spectroscopy. A mixture of CeO_2 NP powder and KBr powder was made into pellets (10 mg of powder/100 mg of KBr) and used for obtaining its FT-IR absorption spectrum in ATR mode on a Bruker ALPHA FT-IR spectrometer in the range of 400−4000 cm^{-1}.

5.7.3. Zeta Potential Studies. A dilute NP suspension prepared by dispersing NPs in water under ultrasonication was used to measure their size and zeta potential using a zetasizer (Nano-ZS, Malvern Instruments).

5.7.4. X-ray Diffraction (XRD) Studies. To perform XRD, CeO_2 NP powder was exposed to Cu Kα radiation with a wavelength (λ) of 1.5408 Å in the 2θ range of 20−100° using a PANalytical X'Pert Pro X-ray diffractometer. The obtained diffraction peaks were compared with the standard JCPDS database.

5.7.5. Scanning Electron Microscopy (SEM). A dilute NP suspension prepared by dispersing NPs in water under ultrasonication was placed on a silicon wafer and air-dried overnight to completely remove any moisture. After sputter coating with a thin layer of gold, the samples were analyzed using a Quanta 200 FEG scanning electron microscope operating at 5 kV to investigate the size, shape, and morphology of the NPs.

5.7.6. Transmission Electron Microscopy (TEM). For sample preparation, 4 μL of dilute NP suspension was placed on carbon-coated copper grids and air-dried overnight to completely remove the moisture. Control NPs and larvae fed with NP-containing cornmeal were imaged under JEOL TEM 2100 Plus (Japan) at an accelerating voltage of 200 kV. For larvae gut imaging, third instar larvae from the control and treatment groups were collected and washed with 1× PBS to remove any food traces, and then, their guts were dissected and a portion of these were transferred onto copper grids for air drying.

5.8. Statistical Analysis. Statistical analysis was performed using GraphPad Prism 6.0, followed by Dunnett's post-test to compare the significance of treatment groups with control. Significance was set to $P < 0.05$. The values expressed are mean ± SEM.

■ ASSOCIATED CONTENT

Supporting Information

The Supporting Information is available free of charge on the ACS Publications website at DOI: 10.1021/acsomega.8b02747.

Size and zeta potential measurements of synthesized cerium oxide NPs (PDF)

■ AUTHOR INFORMATION

Corresponding Author

*E-mail: rsanandhakumar@gmail.com, anandhakumar.s@res.srmuniv.ac.in. Tel.: 914427417902 (Off). Mobile: 919176222654.

ORCID

Anandhakumar Sundaramurthy: 0000-0001-6870-7318

Author Contributions

†Both authors contributed equally to this work.

Notes

The authors declare no competing financial interest.

No ethical clearance was required for research on *Drosophila melanogaster*

■ ACKNOWLEDGMENTS

A.S. acknowledges the financial support from the Department of Science and Technology (DST)−Science and Engineering Research Board (File No. YSS/2015/000771). S.S.M. acknowledges the financial support from the Department of Science and Technology (DST)−Science and Engineering Research Board (File No. ECR/2016/000490).

■ REFERENCES

(1) Matijević, E.; Hsu, W. P. Preparation and properties of monodispersed colloidal particles of lanthanide compounds: I. Gadolinium, europium, terbium, samarium, and cerium (III). *J. Colloid Interface Sci.* **1987**, *118*, 506−523.

(2) Xu, C.; Qu, X. Cerium oxide nanoparticle: a remarkably versatile rare earth nanomaterial for biological applications. *NPG Asia Mater.* **2014**, *6*, No. e90.

(3) Shahin, A. M.; Grandjean, F.; Long, G. J.; Schuman, T. P. Cerium LIII-edge XAS investigation of the structure of crystalline and amorphous cerium oxides. *Chem. Mater.* **2005**, *17*, 315−321.

(4) Tsunekawa, S.; Sahara, R.; Kawazoe, Y.; Kasuya, A. Origin of the blue shift in ultraviolet absorption spectra of nanocrystalline CeO_{2-x} particle. *Mater. Trans. JIM* **2000**, *41*, 1104−1107.

(5) Trovarelli, A.; de Leitenburg, C.; Boaro, M.; Dolcetti, G. The utilization of ceria in industrial catalysis. *Catal. Today* **1999**, *50*, 353−367.

(6) Zhou, F.; Zhao, X.; Xu, H.; Yuan, C. CeO_2 spherical crystallites: synthesis, formation mechanism, size control, and electrochemical property study. *J. Phys. Chem. C* **2007**, *111*, 1651−1657.

(7) Chen, H.-I.; Chang, H.-Y. Synthesis and characterization of nanocrystalline cerium oxide powders by two-stage non-isothermal precipitation. *Solid State Commun.* **2005**, *133*, 593−598.

DOI: 10.1021/acsomega.8b02747
ACS Omega 2019, 4, 104−113

(8) Hirano, M.; Kato, E. Hydrothermal synthesis of nanocrystalline cerium(IV) oxide powders. *J. Am. Ceram. Soc.* **1999**, *82*, 786−788.
(9) Gnanam, S.; Rajendran, V. Synthesis of CeO_2 or α−Mn_2O_3 nanoparticles via sol−gel process and their optical properties. *J. Solgel Sci. Technol.* **2011**, *58*, 62−69.
(10) Bumajdad, A.; Zaki, M. I.; Eastoe, J.; Pasupulety, L. Microemulsion-based synthesis of CeO_2 powders with high surface area and high-temperature stabilities. *Langmuir* **2004**, *20*, 11223−11233.
(11) Sun, C.; Li, H.; Zhang, H.; Wang, Z.; Chen, L. Controlled synthesis of CeO_2 nanorods by a solvothermal method. *Nanotechnology* **2005**, *16*, 1454.
(12) López-Navarrete, E.; Caballero, A.; González-Elipe, A. R.; Ocaña, M. Low-temperature preparation and structural characterization of Pr-doped ceria solid solutions. *J. Mater. Res.* **2002**, *17*, 797−804.
(13) Fisenko, S. P.; Wang, W.-N.; Lenggoro, I. W.; Okyuama, K. Evaporative cooling of micron-sized droplets in a low-pressure aerosol reactor. *Chem. Eng. Sci.* **2006**, *61*, 6029−6034.
(14) Lee, J.-S.; Choi, S.-C. Crystallization behavior of nano-ceria powders by hydrothermal synthesis using a mixture of H_2O_2 and NH_4OH. *Mater. Lett.* **2004**, *58*, 390−393.
(15) Chen, P. L.; Chen, I. W. Reactive cerium (IV) oxide powders by the homogeneous precipitation method. *J. Am. Ceram. Soc.* **1993**, *76*, 1577−1583.
(16) Ketzial, J. J.; Nesaraj, A. S. Synthesis of CeO_2 nanoparticles by chemical precipitation and the effect of a surfactant on the distribution of particle sizes. *J. Ceram. Process. Res.* **2011**, *12*, 74−79.
(17) Zhang, F.; Jin, Q.; Chan, S.-W. Ceria nanoparticles: size, size distribution, and shape. *J. Appl. Phys.* **2004**, *95*, 4319−4326.
(18) Li, M.; Shi, P.; Xu, C.; Ren, J.; Qu, X. Cerium oxide caged metal chelator: anti-aggregation and anti-oxidation integrated H_2O_2-responsive controlled drug release for potential Alzheimer's disease treatment. *Chem. Sci.* **2013**, *4*, 2536−2542.
(19) Alili, L.; Sack, M.; Karakoti, A. S.; Teuber, S.; Puschmann, K.; Hirst, S. M.; Reilly, C. M.; Zanger, K.; Stahl, W.; Das, S.; Seal, S.; Brenneisen, P. Combined cytotoxic and anti-invasive properties of redox-active nanoparticles in tumor-stroma interactions. *Biomaterials* **2011**, *32*, 2918−2929.
(20) Niu, J.; Wang, K.; Kolattukudy, P. E. Cerium oxide nanoparticles inhibits oxidative stress and nuclear factor-κB activation in H9c2 cardiomyocytes exposed to cigarette smoke extract. *J. Pharmacol. Exp. Ther.* **2011**, *338*, 53−61.
(21) Chen, S.; Hou, Y.; Cheng, G.; Zhang, C.; Wang, S.; Zhang, J. Cerium oxide nanoparticles protect endothelial cells from apoptosis induced by oxidative stress. *Biol. Trace. Elem. Res.* **2013**, *154*, 156−166.
(22) Baker, C. H. Harnessing cerium oxide nanoparticles to protect normal tissue from radiation damage. *Transl. Cancer Res.* **2013**, *2*, 343−358.
(23) Alaraby, M.; Hernández, A.; Annangi, B.; Demir, E.; Bach, J.; Rubio, L.; Creus, A.; Marcos, R. Antioxidant and antigenotoxic properties of CeO_2 NPs and cerium sulphate: Studies with Drosophila melanogaster as a promising in vivo model. *Nanotoxicology* **2015**, *9*, 749−759.
(24) Brunner, T. J.; Wick, P.; Manser, P.; Spohn, P.; Grass, R. N.; Limbach, L. K.; Bruinink, A.; Stark, W. J. In vitro cytotoxicity of oxide nanoparticles: comparison to asbestos, silica, and the effect of particle solubility. *Environ. Sci. Technol.* **2006**, *40*, 4374−4381.
(25) Gojova, A.; Lee, J-T.; Jung, H. S.; Guo, B.; Barakat, A. I.; Kennedy, I. M. Effect of cerium oxide nanoparticles on inflammation in vascular endothelial cells. *Inhal. Toxicol.* **2009**, *21*, 123−130.
(26) Patil, S.; Sandberg, A.; Heckert, E.; Self, W.; Seal, S. Protein adsorption and cellular uptake of cerium oxide nanoparticles as a function of zeta potential. *Biomaterials* **2007**, *28*, 4600−4607.
(27) Asati, A.; Santra, S.; Kaittanis, C.; Perez, J. M. Surface-charge-dependent cell localization and cytotoxicity of cerium oxide nanoparticles. *ACS Nano* **2010**, *4*, 5321−5331.
(28) Kos, M.; Kokalj, A. J.; Glavan, G.; Marolt, G.; Zidar, P.; Božič, J.; Novak, S.; Drobne, D. Cerium(IV) oxide nanoparticles induce sublethal changes in honeybees after chronic exposure. *Environ. Sci.: Nano* **2017**, *4*, 2297−3102.
(29) Strawn, E. T.; Cohen, C. A.; Rzigalinski, B. A. Cerium oxide nanoparticles increase lifespan and protect against free radical-mediated toxicity. *FASEB J.* **2006**, *20*, A1356−A1356.
(30) Cohen, C. A.; Karfakis, J. A.; Kurnick, M. D.; Rzigalinski, B. Cerium oxide nanoparticles reduce free radical-mediated toxicity in Drosophila melanogaster. *FASEB J.* **2008**, *22*, 624.1−624.1.
(31) Cohen, C. A.; Kurnick, M. D.; Rzigalinski, B. A. Cerium oxide nanoparticles extend lifespan and protect Drosophila melanogaster from paraquat (PQ)-induced oxidative stress (OS). *Free Radicals Biol. Med.* **2006**, *41*, S20−S20.
(32) D'Angelo, B.; Santucci, S.; Benedetti, E.; Di Loreto, S.; Phani, R. A.; Falone, S.; Amicarelli, F.; Ceru, M. P.; Cimini, A. Cerium oxide nanopartilces trigger neuronal survival in a Human Alzheimer Disease model by modulating BDNF pathway. *Curr. Nanosci.* **2009**, *5*, 167−176.
(33) Estevez, A. Y.; Pritchard, S.; Harper, K.; Aston, J. W.; Lynch, A.; Lucky, J. J.; Ludington, J. S.; Chatani, P.; Mosenthal, W. P.; Leiter, J. C.; Andreescu, S.; Erlichman, J. S. Neuroprotective mechanisms of cerium oxide nanoparticles in a mouse hippocampal brain slice model of ischemia. *Free Radicals Biol. Med.* **2011**, *51*, 1155−1163.
(34) Dillon, C. E.; Billings, M.; Hockey, K. S.; DeLaGarza, L.; Rzigalinski, B. A. Cerium oxide nanoparticles protect against MPTP-induced dopaminergic neurodegeneration in a mouse model for Parkinson's disease. *NSTI-Nanotech.* **2011**, *6*, 451−454.
(35) Liu, X.; Vinson, D.; Abt, D.; Hurt, R. H.; Rand, D. M. Differential toxicity of carbon nanomaterials in Drosophila: larval dietary uptake is benign, but adult exposure causes locomotor impairment and mortality. *Environ. Sci. Technol.* **2009**, *43*, 6357−6363.
(36) Vega-Alvarez, S.; Herrera, A.; Rinaldi, C.; Carrero-Martinez, F. A. Tissue-specific direct microtransfer of nanomaterials into Drosophila embryos as a versatile in vivo test bed for nanomaterial toxicity assessment. *Int. J. Nanomedicine* **2014**, *9*, 2031−2041.
(37) Alaraby, M.; Annangi, B.; Marcos, R.; Hernández, A. Drosophila melanogaster as a suitable in vivo model to determine potential side effects of nanomaterials: A review. *J. Toxicol. Environ. Health. B Crit. Rev.* **2016**, *19*, 65−104.
(38) Glanzman, D. L. Ion pumps get more glamorous. *Nat. Neurosci.* **2010**, *13*, 4.
(39) Yu, X.; Li, F.; Ye, X.; Xin, X.; Xue, Z. Synthesis of cerium (IV) oxide ultrafine particles by solid-state reactions. *J. Am. Ceramic Soc.* **2000**, *83*, 964−966.
(40) Gao, W.; Zhang, Z.; Li, J.; Ma, Y.; Qu, Y. Surface engineering on CeO_2 nanorods by chemical redox etching and their enhanced catalytic activity for CO oxidation. *Nanoscale* **2015**, *7*, 11686−11691.
(41) El Badawy, A. M.; Silva, R. G.; Morris, B.; Scheckel, K. G.; Suidan, M. T.; Tolaymat, T. M. Surface charge-dependent toxicity of silver nanoparticles. *Environ. Sci. Technol.* **2010**, *45*, 283−287.
(42) Feng, Q.; Liu, Y.; Huang, J.; Chen, K.; Huang, J.; Xiao, K. Uptake, distribution, clearance, and toxicity of iron oxide nanoparticles with different sizes and coatings. *Sci. Rep.* **2018**, *8*, 2082.
(43) Di Bona, K. R.; Xu, Y.; Ramirez, P. A.; DeLaine, J.; Parker, C.; Bao, Y.; Rasco, J. F. Surface charge and dosage dependent potential developmental toxicity and biodistribution of iron oxide nanoparticles in pregnant CD-1 mice. *Reprod. Toxicol.* **2014**, *50*, 36−42.
(44) Nichols, C. D.; Becnel, J.; Pandey, U. B. Methods to assay Drosophila behaviour. *J. Visualized Exp.* **2012**, 3795.

DOI: 10.1021/acsomega.8b02747
ACS Omega 2019, 4, 104−113